MATHEMATICAL MODELING OF CZOCHRALSKI TYPE GROWTH PROCESSES FOR SEMICONDUCTOR BULK SINGLE CRYSTALS[1]

Wolfgang Dreyer[2], Pierre-Étienne Druet[2], Olaf Klein[2], Jürgen Sprekels[2]

Abstract

This paper deals with the mathematical modeling and simulation of crystal growth processes by the so-called *Czochralski method* and related methods, which are important industrial processes to grow large bulk single crystals of semiconductor materials such as, e. g., gallium arsenide (GaAs) or silicon (Si) from the melt. In particular, we investigate a recently developed technology in which *traveling magnetic fields* are applied in order to control the behavior of the turbulent melt flow. Since numerous different physical effects like electromagnetic fields, turbulent melt flows, high temperatures, heat transfer via radiation, etc., play an important role in the process, the corresponding mathematical model leads to an extremely difficult system of initial-boundary value problems for nonlinearly coupled partial differential equations. In this paper, we describe a mathematical model that is under use for the simulation of real-life growth scenarios, and we give an overview of mathematical results and numerical simulations that have been obtained for it in recent years.

1 Introduction

Large bulk single crystals of semiconducting materials like, e. g., gallium arsenide (GaAs), germanium (Ge), and silicon (Si), form an indispensable prerequisite for modern electronic and optical technologies. Entire industries depend on the availability of semiconductor single crystals. It is therefore of utmost technological importance to develop and improve effective and cheap industrial growth methods.

The most important industrial techniques for growing bulk semiconductor are the *Czochralski growth(Cz)*, the *vapor pressure controlled Czochralski growth (VCz)*, and the *liquid encapsulated Czochralski growth (LEC)*. In this paper, we will use the notion *Czochralski type* to describe any of these growth processes and related ones. In the growth processes of Czochralski type, a rotating crystal seed is dipped into the molten semiconductor material, which is contained in a crucible that rotates in the opposite direction. The seed is then slowly pulled out of the melt, and a single crystal solidifies.

A typical growth apparatus is depicted in Fig. 1; here, the left side shows the geometry, while the right side shows the temperature distribution during a growth run calculated with the software package `WIAS-HiTNIHS` developed at the Weierstrass Institute for Applied Analysis

[1]This papers combines results that were derived in project C9 of the DFG Research Center MATHEON in Berlin and in the project KRIST $\widetilde{MAG}^{®}$, which was supported by the German Federal State of Berlin in the framework of the "Zukunftsfonds Berlin" in the TSB Technologiestiftung Berlin and by the German Federal State of Brandenburg. The latter project was co-financed by the European Union within the European Regional Development Fund (EFRE).

[2]Weierstrass Institute, Mohrenstr. 39, 10117 Berlin, Germany, e-mail: wolfgang.dreyer@wias-berlin.de, pierreetienne.druet@wias-berlin.de, olaf.klein@wias-berlin.de, juergen.sprekels@wias-berlin.de

and Stochastics (WIAS) in Berlin.

For many growth processes of Czochralski type, the melt flow is turbulent, which creates the problem that impurities can find their way into the crystal, lowering its quality. Also, crystal growers want the solid-liquid interface to have a certain shape, and the temperature oscillations below the crystal should have small amplitudes and not too small frequencies.

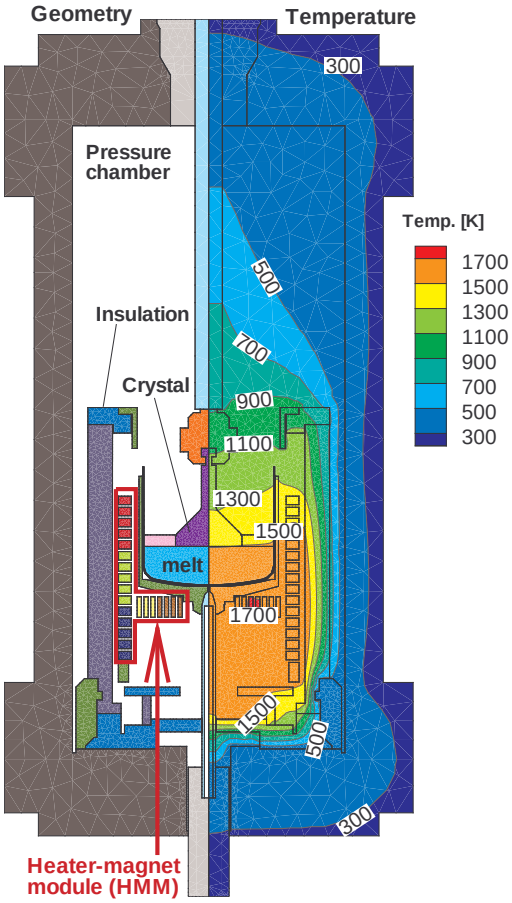

Figure 1: Left-hand side: Configuration of Czochralski furnace; right-hand side: Temp. field computed by WIAS-HiTNIHS. For details, see section 4.

Since the melt is electrically conducting, electromagnetic fields can play the role of a *control*, since a Lorentz force is induced into the melt in their presence. In the past, time-dependent magnetic fields were successfully applied to improve crystal growth processes from the melt. Typically, the magnetic fields were generated by magnets or induction coils placed *outside* of the growth apparatus. However, with this kind of configuration it requires much energy to produce a magnetic field of sufficient magnitude in the melt, especially in cases when the thick walls of the pressure chamber shield the magnetic field significantly (e. g., in the growth of III–V compounds with the LEC or VCz processes). In the project KRIST $\widetilde{MAG}^{®}$, an internal heater-magnet module (HMM) has been developed, which consists of several coils that operate as a resistance heater while simultaneously generating a traveling magnetic field (TMF). It was demonstrated that this HMM can produce appropriate magnetic fields in the melt with moderate power consumption, see [15, 20, 24, 25].

An important role for the success of the KRIST $\widetilde{MAG}^{®}$ project played *mathematical modeling and simulation*. In this contribution, we give an overview of the mathematical model that was used to solve the problem, and we report on some theoretical and numerical results that were obtained.

The paper is organized as follows: in Section 2 we discuss the main physical effects that occur in processes of Czochralski type under the influence of traveling magnetic fields, and we describe the mathematical model. Section 3 brings a number of mathematical results that have been proved for various aspects of the general problem; here, we deal with problems like well-posedness, regularity, and optimal control of the model equations (or of appropriate simplified versions thereof). In the final Section 4 we present some results of numerical simulations obtained for real-life configurations, namely the LEC crystal growth of GaAs.

2 A mathematical model for processes of Czochralski type

2.1 Processes of Czochralski type and TMFs

The single crystal growth processes of Czochralski type are technologically complicated. Quality and size of the grown crystals are influenced by a number of parameters that act on very different time and space scales.

Global variables on the *macroscale*, which are important in the whole apparatus (and beyond) are the temperature field and the electromagnetic field. On the *intermediate scale*, locally within the crucible, we have the velocity field of the melt flow and the concentrations of impurities (e. g., oxygen, nitrogen, silicon carbide, silicon nitride) that should not be incorporated in the crystal. Moreover, the free boundary between melt and solidified crystal should have a certain (convex) shape in order that perfect single crystals grow. A problem on the *microscale* of a few millimeters is the interaction between melt and container wall, which influences the shape of the interface in the close vicinity of the wall.

Another problem, this time a temporal one, is given by the fact that the turbulent melt flow induces temporal oscillations of the melt temperature below the growing crystal; these oscillations should have a small amplitude and a high frequency in order that the solid-liquid interface have no time to react to their occurrence. Using a TMF to improve the melt flow during crystal growth processes requires practical and theoretical investigations.

From the mathematical point of view, the following facts complicate analysis and simulation:

– due to temperatures of up to $2000\ K$, many of the physical coefficients depend on temperature,
– physical coefficients and boundary conditions jump between the different materials of the growth apparatus,
– the geometry of the apparatus is very complex and multiscale,
– the main energy transport in the gas cavities is due to radiation.

The latter complication presents a particular challenge, since it leads to both nonlocal and nonlinear boundary conditions for the temperature in the gas cavities.

In the following, we describe the mathematical model that was used in the project. Here, we follow closely the exposition in [6].

2.2 Geometry of the problem

We denote by $\Omega \subset \widetilde{\Omega} \subset \mathbb{R}^3$ two bounded domains[3], which respectively represent the region of interest for the computation of the temperature and of the electromagnetic field. In our case, Ω, whose boundary is denoted by Γ, represents the furnace depicted in Fig. 1. The domain $\widetilde{\Omega}$

[3] Here, and throughout the paper, a domain is a connected open set.

has the form

$$\overline{\widetilde{\Omega}} = \bigcup_{i=0}^{m} \overline{\widetilde{\Omega}_i}, \quad \text{where } \widetilde{\Omega}_i, \quad i = 0, \dots, m,$$

denote disjoint domains that represent materials having heterogeneous electromagnetic and thermodynamic properties. Setting $\Omega_i := \widetilde{\Omega}_i \cap \Omega$ for $i = 0, \dots, m$, we have $\overline{\Omega} = \bigcup_{i=0}^{m} \overline{\Omega_i}$. We further denote by $\widetilde{\Omega}_c$ the set containing the electrical conductors of the whole system, and we set $\Omega_c := \widetilde{\Omega}_c \cap \Omega$. By $\widetilde{\Omega}_{nc}$, Ω_{nc}, we denote the complements of these sets with respect to $\widetilde{\Omega}$ and Ω.

Let $T > 0$ the final time of the process. We further denote:

$$\begin{aligned} Q &:= (0,T) \times \Omega, \qquad & Q_i &:= (0,T) \times \Omega_i, \quad \text{for } i = 0, \dots, m\,, \\ \widetilde{Q} &:= (0,T) \times \widetilde{\Omega}, \qquad & \widetilde{Q}_i &:= (0,T) \times \widetilde{\Omega}_i, \quad \text{for } i = 0, \dots, m\,. \end{aligned}$$

2.3 The fluiddynamical problem

The liquid semiconducting melt is confined in the bounded domain $\Omega_1 \subset \Omega$ within the crucible. We assume that the liquid obeys the Navier-Stokes equations for an incompressible, viscous and electrically conducting fluid,

$$\rho_1 \left(\frac{\partial v}{\partial t} + (v \cdot \nabla) v \right) = -\nabla p + \operatorname{div}(\eta(\theta)\, D\, v) + f + j \times B\,, \tag{2.1}$$

$$\operatorname{div} v = 0\,, \qquad \text{in } (0,T) \times \Omega_1\,, \tag{2.2}$$

where ρ_1 is the reference density of the fluid, η its viscosity, f the gravitational force, and $j \times B$ the Lorentz force. Here and throughout the paper, we use the notations

$$Dv := (D_{i,j}(v))\,, \quad \text{where } D_{i,j}(v) := \frac{1}{2} \left(\frac{\partial v_i}{\partial x_j} + \frac{\partial v_j}{\partial x_i} \right) \quad \text{for } 1 \le i, j \le 3\,,$$

$$D(u,\, v) := Du \,:\, Dv := \sum_{i,j=1}^{3} D_{i,j}(u)\, D_{i,j}\,(v)\,.$$

Since the flow is buoyancy-driven, thermal expansion must be accounted for, and we set

$$\rho = \rho(\theta) = \rho_1 \left(1 - \alpha\,(\theta - \theta_1)\right), \tag{2.3}$$

where ρ denotes the mass density of the fluid, α its thermal expansion coefficient, θ is the absolute temperature, and θ_1 a reference temperature.

The gravitational force f is given by

$$f = f(\theta) = \rho(\theta)\, \vec{g}\,, \tag{2.4}$$

where $\vec{g}$ is the fixed vector of gravity. The modeling assumptions (2.3) and (2.4), in combination with (2.2), are constitutive for *Boussinesq's approximation* in the setting of the low Mach-number limit of compressible fluids.

At the boundary, we assume that the velocity is imposed, that is,

$$v = v_g \quad \text{on } (0,T) \times \partial\Omega_1\,, \quad v_g \cdot \vec{n} = 0 \quad \text{on } (0,T) \times \partial\Omega_1\,, \tag{2.5}$$

where $\vec{n}$ is the outward-pointing normal to $\partial\Omega_1$, and " $\cdot$ " stands for the standard euclidean scalar product in $\mathbb{R}^3$. Moreover, at time zero, a velocity distribution v_0 is prescribed,

$$v(0) = v_0 \quad \text{in } \{0\} \times \Omega_1\,. \tag{2.6}$$

2.4 The heat transfer problem

In accordance with the Boussinesq approach, we assume that the dissipative heating due to viscous friction and to the Joule effect is negligible in the fluid. Therefore, assuming that heat convection is significant only in Ω_1, we have

$$\rho_1\, c_{V1} \left(\frac{\partial \theta}{\partial t} + v \cdot \nabla\theta \right) = \operatorname{div}(\kappa(\theta)\, \nabla\theta) \quad \text{in } (0,T) \times \Omega_1\,, \tag{2.7a}$$

$$\rho_i\, c_{Vi} \frac{\partial \theta}{\partial t} = \operatorname{div}(\kappa_i(\theta)\, \nabla\theta) + \frac{|j|^2}{\mathfrak{s}(\theta)} \quad \text{in } (0,T) \times \Omega_i\,, \ \text{for } \Omega_i \subset (\Omega_c \setminus \Omega_1)\,, \tag{2.7b}$$

$$\rho_i\, c_{Vi} \frac{\partial \theta}{\partial t} = \operatorname{div}(\kappa_i(\theta)\, \nabla\theta) \quad \text{in } (0,T) \times \Omega_i\,, \ \text{for } \Omega_i \subset \Omega_{nc}\,, \tag{2.7c}$$

where ρ_i, c_{Vi}, and κ_i denote density, specific heat, and thermal conductivity of the corresponding material, in that order, and θ, $\mathfrak{s}$, and j denote absolute temperature, electrical conductivity, and current density, in that order.

At the high temperatures occurring in crystal growth, heat transport due to radiation is of prime importance. To describe this effect, we assume that the domain $\Omega_0 \subset \Omega$ represents the cavity filled with transparent material. The sets $\Omega_1, \ldots, \Omega_m$ represent diffuse grey, opaque materials. The cavity Ω_0 is enclosed in Ω in the sense that

$$\mathbb{R}^3 \setminus \bigcup_{i=1}^{m} \overline{\Omega_i} \quad \text{is disconnected.} \tag{2.8}$$

The surface $\Sigma := \partial\Omega_0$, the boundary of the transparent enclosed cavity, is nonconvex and possibly disconnected. We use the notation $\mathcal{S} := (0,T) \times \Sigma$.

The heat radiation at Σ is described by a standard model in crystal growth ([19, 18]), namely the boundary condition

$$\left[-\kappa(\theta)\, \frac{\partial \theta}{\partial \vec{n}} \right] = R - J \quad \text{on } (0,T) \times \Sigma\,. \tag{2.9}$$

Here, R is the radiosity, J the incoming radiation, $\vec{n}$ the unit normal pointing inwards to Ω_0, and the symbol $[\,\cdot\,]$ denotes the jump of a quantity across Σ. In order to model R and J, we need to introduce on $\Sigma \times \Sigma$ the so-called *view factor*, which is given by

$$w(z,y) := \begin{cases} \dfrac{\vec{n}(z) \cdot (y-z)\ \vec{n}(y) \cdot (z-y)}{\pi |y-z|^4}\, V(z,y) & \text{if } z \neq y\,, \\ 0 & \text{if } z = y\,, \end{cases} \tag{2.10}$$

where V is the *visibility function* that penalizes the presence of opaque obstacles, given by

$$V(z,y) = \begin{cases} 1 & \text{if conv}\{z,y\} \subset \Omega_0 \cup \{z,y\}\,, \\ 0 & \text{otherwise.} \end{cases}$$

In this connection, the set $\operatorname{conv}\{z,y\} = \{(1-\lambda)z + \lambda y \,|\, \lambda \in [0,1]\}$ denotes the convex hull of the points z, y. The unknown functions $R,\ J$ are connected through the relations

$$R = \epsilon\,\sigma\,\theta^4 + (1-\epsilon)\,J\,, \quad J = K(R), \quad \text{on } (0,T)\times\Sigma\,,$$

that is, R solves the so-called *radiosity equation*

$$(I - (1-\epsilon)\,K)(R) = \sigma\,\epsilon\,\theta^4 \quad \text{on } (0,T)\times\Sigma\,. \tag{2.11}$$

Here, σ is the Stefan-Boltzmann constant, and ϵ denotes the given emissivity of the surface Σ. The linear integral operator K is defined by

$$(K(f))(t,z) := \int_\Sigma w(z,y)\,f(t,y)\,dS_y \quad \text{for } (t,z)\in(0,T)\times\Sigma\,. \tag{2.12}$$

Under mild assumptions on the function ϵ and the regularity of the surface Σ, the solution operator of the equation (2.11) is well-defined (see Thm. 2.4 in [11] for a sharp result). One can therefore introduce an operator G by

$$G := (I-K)\,(I-(1-\epsilon)\,K)^{-1}\,\epsilon\,, \tag{2.13}$$

and equivalently reformulate the conditions (2.9) and (2.11) as

$$\left[-\kappa(\theta)\,\frac{\partial\theta}{\partial\vec{n}}\right] = G(\sigma\,\theta^4) \quad \text{on } (0,T)\times\Sigma\,. \tag{2.14}$$

For further details concerning the boundary condition (2.14), the reader can consult one of the references ([17, 19]).

On the outer boundary $(0,T)\times\Gamma$, we consider the condition

$$\theta = \theta_g \ \text{ on } (0,T)\times\Gamma\,. \tag{2.15}$$

On the other boundaries, we simply assume that the conductive heat flux is continuous. Moreover, we have at time zero

$$\theta(0) = \theta_0 \quad \text{in } \{0\}\times\Omega\,. \tag{2.16}$$

We complement the system (2.7) by the boundary conditions (2.9) and (2.15), and by the initial condition (2.16).

2.5 The electromagnetic problem

To describe the electromagnetic phenomena originating from the heating system and from the applied magnetic fields, we introduce some further notation.

We denote by $\widetilde{\Omega}_{c_0} \subset \widetilde{\Omega}_c$ the conductors where current is applied, which is typically the system that supplies the furnace with current, resp. the conductors that serve to generate a magnetic field. We assume for simplicity that apart from $\widetilde{\Omega}_{c_0}$, the region $\widetilde{\Omega} \setminus \Omega$ consists only of vacuum.

We consider the low-frequency, i.e., diffusive approximation of Maxwell's equations with applied current, described for example in the textbook [1]. The electric field E and the magnetic induction B satisfy Faraday's law of induction

$$\operatorname{curl} E + \frac{\partial B}{\partial t} = 0\,, \quad \text{in } (0,T) \times \widetilde{\Omega}\,. \tag{2.17}$$

Putting the local density of free charges to zero in the nonconducting parts, the electrical displacement D satisfies

$$\operatorname{div} D = 0 \ \text{ in } (0,T) \times \widetilde{\Omega}_{nc}\,. \tag{2.18}$$

The magnetic induction B satisfies

$$\operatorname{div} B = 0 \quad \text{in } (0,T) \times \widetilde{\Omega}\,. \tag{2.19}$$

We need a constitutive relation between B and H, as well as between E and D. We consider only linear materials, that is, we assume that

$$B = \mu\, H, \quad D = \mathfrak{e}\, E \quad \text{in } (0,T) \times \widetilde{\Omega}\,, \tag{2.20}$$

where μ and $\mathfrak{e}$, respectively, denote magnetic permeability and electrical permittivity. Finally, we have to take into account Ampère's law,

$$\operatorname{curl} H = j \quad \text{in } (0,T) \times \widetilde{\Omega}\,, \tag{2.21}$$

as well as Ohm's law in the conductors,

$$j = \mathfrak{s}(\theta)\,(E + v \times B) \quad \text{in } (0,T) \times \widetilde{\Omega}_c\,. \tag{2.22}$$

It remains to model the presence of a current source in the conductors $\widetilde{\Omega}_{c_0}$. Observe that from (2.17) and (2.19) it follows that

$$E = -\frac{\partial A}{\partial t} + \nabla \chi\,,$$

with a magnetic potential A of the magnetic induction B, and a scalar potential χ. In our model, we assume that only the current $\mathfrak{s}\,\nabla\chi$ originating from an applied voltage can be considered as imposed, and we write

$$\mathfrak{s}\,\nabla\chi \approx j_g \quad \text{in } (0,T) \times \widetilde{\Omega}_{c_0}\,,$$

with the given current density j_g. It follows that (2.21) and (2.22) have to be written in the form

$$\operatorname{curl} H = \mathfrak{s}(\theta)\,\left(-\frac{\partial A}{\partial t} + v \times B\right) + j_g\,, \tag{2.23}$$

with $j_g \neq 0$ only in $(0,T) \times \widetilde{\Omega}_{c_0}$. The potential A is related to B by the identity $\operatorname{curl} A = B$, and its choice can be fixed, for example, by requiring the gauge $\operatorname{div} A = 0$.

The boundary conditions for these fields are the *natural interface conditions*

$$\big[H \times \vec{n}\big]_{i,j} = 0\,, \quad \big[B \cdot \vec{n}\big]_{i,j} = 0\,, \quad \big[E \times \vec{n}\big]_{i,j} = 0 \quad \text{on } (0,T) \times (\partial\widetilde{\Omega}_i \cap \partial\widetilde{\Omega}_j)\,, \tag{2.24}$$

where $\big[\,\cdot\,\big]_{i,j}$ denotes the jump of a quantity across the surface $(0,T) \times (\partial\widetilde{\Omega}_i \cap \partial\widetilde{\Omega}_j)$, $i,j = 0,\ldots,m$, $i \neq j$. We consider that the outer boundary can be modeled as a magnetic shield and set

$$B \cdot \vec{n} = 0\,, \quad E \times \vec{n} = 0 \ \text{ on } (0,T) \times \partial\widetilde{\Omega}\,. \tag{2.25}$$

Finally, we impose the initial condition

$$H(0) = 0 \quad \text{in } \{0\} \times \widetilde{\Omega}\,. \tag{2.26}$$

2.6 The full problem

We define the problem **(P)** as the problem of finding a vector field v and a function p in $(0,T) \times \Omega_1$, vector fields H, B, E, D, j in $(0,T) \times \widetilde{\Omega}$ and a nonnegative function θ in $(0,T) \times \Omega$ such that the relations (2.1), (2.2), (2.7), (2.17), (2.18), (2.19), (2.20), (2.23) together with the boundary conditions (2.5), (2.14), (2.15), (2.24), (2.25) and the initial conditions (2.6), (2.16) and (2.26) are satisfied.

In the following sections, we will study various aspects of problem **(P)**.

Remark. 1. The above model is still incomplete, since it ignores the presence of the solid-liquid interface.

2. We have not accounted for the presence of impurities in the melt flow.

3. We have restricted our model to the macro- and intermediate scales; effects on the microscale such as the interaction between solid-liquid interface and the container wall are neglected.

4. The heat flux by gas convection in the cavity is ignored as well.

3 Existence, uniqueness and optimal control

The existence of weak solutions to the model described in the section 2.1 was first investigated in the doctoral thesis [6]. Uniqueness statements could also be proved, but only for classical solutions, which is typical for Navier-Stokes systems. In [5], some aspects of the existence proof could be simplified. We will briefly discuss the essentials of these results in subsection 3.1 below.

A second direction of investigations concerns the optimal control of the PDE system. The main relevant control parameters for the real problem are the current source j_g in the conductors $\widetilde{\Omega}_{c_0}$ (cf. (2.23)) and the velocity v_g imposed on the boundary $\partial\Omega_1$ of the fluid (cf. (2.5)). The state to be optimized is primarily the temperature θ, either in the entire apparatus or locally, in the vicinity of the crystal. Obviously, also the velocity of the fluid v and the magnetic field

H are of interest. In a first attempt, we tried to derive first-order optimality conditions for the control-to-state mapping under pointwise state constraints for the temperature. It turned out that a drastic simplification of the real model is necessary to follow this approach. Nevertheless, we were able to make significant analytical progress in [10], which we are going to resume below in the second subsection 3.4.

3.1 The weak solution approach

Recall that j and B are related to H via the linear relations (2.20) and (2.21), respectively. Let v satisfy the equations (2.1) and (2.2). It is well known that, for all $\phi \in [C_c^\infty([0,T)\times\Omega_1)]^3$ such that $\operatorname{div}\phi(t) = 0$ in Ω_1 for all $t \in [0,T)$, we have the integral relation

$$\begin{aligned} &-\int_{Q_1} \rho_1\, v\cdot\frac{\partial\phi}{\partial t} + \int_{Q_1} \rho_1\,(v\cdot\nabla)v\cdot\phi + \int_{Q_1} \eta(\theta)\, D(v\,,\,\phi) \\ &= \int_{\Omega_1} v_0\cdot\phi(0) + \int_{Q_1} (\operatorname{curl} H\times\mu\, H)\cdot\phi + \int_{Q_1} f(\theta)\cdot\phi\,, \end{aligned} \tag{3.1}$$

where the unknown pressure p does no longer occur. Now assume that H and E satisfy the relation (2.17) and the modeling assumption (2.23). Then it holds, for all $\psi \in C_c^\infty([0,T)\times\widetilde{\Omega})]^3$ such that $\operatorname{curl}\psi(t) = 0$ in the nonconductors $\widetilde{\Omega}_{nc}$ for all $t \in [0,T)$, the relation

$$\begin{aligned} &-\int_{\widetilde{Q}} \mu\, H\cdot\frac{\partial\psi}{\partial t} + \int_{\widetilde{Q}_c} \mathfrak{s}^{-1}(\theta)\,\operatorname{curl} H\cdot\operatorname{curl}\psi \\ &= \int_{Q_1} \big(v\times\mu\, H\big)\cdot\operatorname{curl}\psi \,+ \int_{\widetilde{Q}_c} \mathfrak{s}^{-1}(\theta)\, j_g\cdot\operatorname{curl}\psi, \end{aligned} \tag{3.2}$$

where the magnetic field strength H is the only remaining unknown.

Assume that the (reference) mass density ρ_1 of the fluid is a given constant, and assume that there exist positive constants $\mathfrak{s}_l$, $\mathfrak{s}_u$, μ_l, μ_u, κ_l, κ_u, η_l, η_u such that

$$\begin{gathered} 0 < \mathfrak{s}_l \le \mathfrak{s} \le \mathfrak{s}_u < +\infty\,, \quad 0 < \mu_l \le \mu \le \mu_u < +\infty\,, \\ 0 < \eta_l \le \eta \le \eta_u < +\infty\,. \end{gathered} \tag{3.3}$$

It is possible to choose $\phi = v - v_g$ in (3.1) and $\psi = H$ in (3.2). Standard inequalities yield the *a priori* estimate

$$\begin{aligned} &\int_{Q_1} \eta(\theta)\, D(v,v) + \int_{\widetilde{Q}_c} \mathfrak{s}^{-1}(\theta)\,|\operatorname{curl} H|^2 \\ &\le C\,\Big(\|v_g\|^2_{W_2^1(Q_1)} + \|v_g\|^2_{L^\infty(Q_1)} + \|j_g\|^2_{L^2(\widetilde{Q}_{c_0})} + \|f(\theta)\|^2_{L^2(Q_1)}\Big)\,. \end{aligned} \tag{3.4}$$

In (3.4), the constant C depends on the constants of condition (3.3) and on the structure of Ω_1. In order to obtain a *uniform* estimate for the MHD energy on the left-hand side of (3.4), it is therefore sufficient to assume that

$$v_g \in [W_2^1(Q_1)]^3 \cap [L^\infty(Q_1)]^3, \quad j_g \in [L^2(\widetilde{Q}_{c_0})]^3\,, \tag{3.5}$$

$$f \in [L^\infty(\mathbb{R})]^3\,. \tag{3.6}$$

While the conditions (3.5) are completely natural, the restriction (3.6) is more demanding, since it is actually incompatible with the linear model (2.3), (2.4). Another option that keeps (2.3) untouched, but leads to a higher mathematical technicality in the proofs, is to treat the thermal expansion coefficient α as a small perturbation.

Next, we take a look at the heat equation (2.7). We deduce in a standard way that for all $\xi \in C_c^\infty([0,T)\times\Omega)$ it holds

$$
\begin{aligned}
&-\int_Q \rho\, c_V\, \theta\, \frac{\partial \xi}{\partial t} - \int_{Q_1} \rho_1\, c_{V1}\, \theta\, v\cdot\nabla\xi + \int_Q \kappa(\theta)\nabla\theta\cdot\nabla\xi + \int_S G(\sigma\,\theta^4)\,\xi \\
&= \int_\Omega \theta_0\,\xi(0) + \int_{Q_c\setminus Q_1} \mathfrak{s}^{-1}(\theta)\,|\operatorname{curl} H|^2\,\xi\,. \qquad (3.7)
\end{aligned}
$$

In the analysis of (3.7), the following difficulty arises: if the estimate (3.4) is the best we can obtain for $\operatorname{curl} H$ then the right-hand side of the heat equation belongs to at most L^1. Under the assumptions that the specific heat c_{V1} of the fluid is a constant, and that there are constants κ_l, κ_u such that

$$0 < \kappa_l \le \kappa \le \kappa_u < +\infty,$$

we can expect from general techniques for parabolic systems with right-hand sides in L^1 a bound for $\nabla\theta$ in $L^p(Q)$, but only for the range $1 \le p < 5/4$. This is far away from being sufficient to control the radiation energy that grows like $\|\theta\|_{L^4(S)}$.

Note, in addition, that the mentioned techniques are even not designed for the case of nonlocal and nonlinear radiation boundary conditions. In this context, an important part of our effort was dedicated to obtaining an *a priori* bound for θ in $L^4(S)$ (see [9]). Here, we need to impose on the surface Σ where radiation takes place the restriction that

$$\Sigma \in \mathcal{C}^{1,\alpha},\ \ \alpha \in (0,1]\,, \qquad (3.8)$$

which ensures the compactness of the integral operator K (cf. (2.12)) in $L^p(\Sigma)$. Moreover, it is required for the emissivity ϵ (cf. (2.11)) that

$$0 < \epsilon_l \le \epsilon \le \epsilon_u < 1 \quad \text{ on } \Sigma\,. \qquad (3.9)$$

This condition, while excluding the presence of white and of black bodies in the apparatus, guarantees a minimal coercivity of the operator G defined in (2.13).

To prove the existence of weak solutions, one needs to construct a solvable approximation of the PDE system such that the *a priori* estimate (3.4) and the radiation bound are preserved. In [5], a truncation approach for the quadratic nonlinearities of the system proved to be successful. In the passage to the limit as the approximation parameter $\delta > 0$ approaches zero, another important problem occurs, since no compactness is available for the sequence $\{|\operatorname{curl} H_\delta|^2\}$. Therefore, the approximation scheme converges, but only to a weak solution *with defect measure*. This means that, instead of the heat equation (3.7), the weak solution satisfies

$$
\begin{aligned}
&-\int_Q \rho\, c_{V1}\, \theta\, \frac{\partial \xi}{\partial t} - \int_{Q_1} \rho_1\, c_{V1}\, \theta\, v\cdot\nabla\,\xi + \int_Q \kappa(\theta)\nabla\theta\cdot\nabla\xi + \int_S G(\sigma\,\theta^4)\,\xi \\
&= \int_\Omega \theta_0\,\xi(0) + \int_{Q_c\setminus Q_1} \mathfrak{s}^{-1}(\theta)\,|\operatorname{curl} H|^2\,\xi + \int_{[0,T]\times\partial\Omega_c} \xi\, d\,\bar{\nu}\,. \qquad (3.10)
\end{aligned}
$$

Here, $\bar{\nu} \in \mathcal{M}(\overline{Q})$ is a Borel regular, *positive* Radon measure concentrated in the set $[0,T] \times \partial\Omega_c$.

In order to precisely state the definition of a weak solution and the existence theorem, we now introduce or recall the definition of some functional spaces. For $1 \leq q \leq \infty$, we introduce the space

$$L^q_{\mathsf{curl}}(\tilde{\Omega}) := \left\{ H \in [L^q(\tilde{\Omega})]^3 \,\middle|\, \operatorname{curl} H \in [L^q(\tilde{\Omega})]^3 \right\}, \tag{3.11}$$

where the differential operator *curl* has to be understood in its generalized sense. It is well known that $L^2_{\mathrm{curl}}(\widetilde{\Omega})$ is a Hilbert space with respect to the inner product

$$(H_1\,,\, H_2)_{L^2_{\mathrm{curl}}(\widetilde{\Omega})} := \int_{\widetilde{\Omega}} (\operatorname{curl} H_1 \cdot \operatorname{curl} H_2 + H_1 \cdot H_2),$$

and that $L^q_{\mathrm{curl}}(\widetilde{\Omega})$ is a Banach space when endowed with the graph norm.

To represent currents, we need spaces of vector fields that vanish in the nonconductors, namely

$$\mathcal{H}^q(\widetilde{\Omega}) := \left\{ H \in L^q_{\mathrm{curl}}(\widetilde{\Omega}) \,\middle|\, \operatorname{curl} H = 0 \text{ in } \widetilde{\Omega}_{nc} \right\}. \tag{3.12}$$

These spaces are closed linear subspaces of $L^q_{\mathrm{curl}}(\widetilde{\Omega})$. Moreover, the space $\mathcal{H}(\widetilde{\Omega}) := \mathcal{H}^2(\widetilde{\Omega})$ is a Hilbert space.

It is possible to deal with the divergence constraint (2.19) and with the boundary conditions (2.25) by introducing the space

$$\mathcal{H}_\mu(\widetilde{\Omega}) := \left\{ H \in \mathcal{H}(\widetilde{\Omega}) \,\middle|\, \operatorname{div}(\mu\, H) = 0 \text{ in } \widetilde{\Omega}\,;\ \mu\, H \cdot \vec{n} = 0 \text{ on } \partial\widetilde{\Omega} \right\}, \tag{3.13}$$

where the divergence constraint and the boundary condition are also intended in the sense of the generalized div operator. In general, we denote by the subscript μ spaces of vectors satisfying the (weak) constraints $\operatorname{div}(\mu\, H) = 0$ (with respect to $\widetilde{\Omega}$) and $\mu\, H \cdot \vec{n} = 0$ (with respect to $\partial\widetilde{\Omega}$).

In connection with the Navier-Stokes equations, we need the usual spaces

$$D^{1,q}(\Omega_1) := \left\{ u \in [W^{1,q}(\Omega_1)]^3 \,\middle|\, \operatorname{div} u = 0 \text{ a. e. in } \Omega_1 \right\},$$

$$D^{1,q}_0(\Omega_1) := \left\{ u \in [W^{1,q}_0(\Omega_1)]^3 \,\middle|\, \operatorname{div} u = 0 \text{ a. e. in } \Omega_1 \right\}.$$

For $1 \leq p < \infty$, we use the Sobolev spaces

$$W^{1,0}_p(Q) := \left\{ u \in L^p(Q) \,\middle|\, \exists\, u_{x_i} \in L^p(Q)\ (i = 1,\, 2,\, 3) \right\},$$

$$W^1_p(Q) := \left\{ u \in W^{1,0}_p(Q) \,\middle|\, \exists\, u_t \in L^p(Q) \right\},$$

where all partial derivatives are to be understood in the weak sense. In connection with heat radiation, we define for $1 \le p < \infty$, $4 \le q \le \infty$, the spaces

$$\mathcal{V}_0^{p,q}(Q) := \left\{ u \in W_p^{1,0}(Q) \,\middle|\, \text{trace}\, u \in L^q(\mathcal{S}) \right\},$$

$$\mathcal{V}^{p,q}(Q) := \left\{ u \in W_p^{1}(Q) \,\middle|\, \text{trace}\, u \in L^q(\mathcal{S}) \right\}.$$

Here, we have used the abbreviation $\mathcal{S} := (0,T) \times \Sigma$. In analogy to (3.11), we can define the spaces $L^q_{\mathrm{curl}}(\widetilde{Q})$, and referring to (3.12), (3.13), we introduce the spaces $\mathcal{H}_q(\widetilde{Q})$, $\mathcal{H}_\mu(\widetilde{Q})$. If we require a q-integrable partial derivative with respect to time then we write $\mathcal{H}^1_q(\widetilde{Q})$, $\mathcal{H}^1_\mu(\widetilde{Q})$.

Next, we define $D_q^{1,0}(Q_1)$ (resp. $D_q^1(Q_1)$) to be the subspace of $[W_q^{1,0}(Q_1)]^3$ (resp. $[W_q^1(Q_1)]^3$) that contains all elements having an almost everywhere vanishing divergence. Using the subscript $\mathcal{C}$, we denote subspaces of functions that vanish on the surface $]0\,,\,T[\times\Gamma$. We sometimes abuse notation and denote spaces of both scalar and vector variables by the same symbols L^p, respectively, $W_p^{1,0}$.

We are now ready to technically define the notion of a weak solution: in fact, it can be verified as in [5], using various embedding relations of Sobolev-type, that all duality pairings occurring in the relations (3.1), (3.2), and (3.10) are finite for the following classes of solution and testfunctions.

Definition 3.1 (Weak solution with defect measure) *Suppose that the triple* $\{v,\, H,\, \theta\}$ *belongs to the space*

$$\Big[D_2^{1,0}(Q_1) \times \mathcal{H}_\mu(\widetilde{Q}) \cap \times \bigcap_{1\le p<5/4} \mathcal{V}_0^{p,4}(Q) \Big] \cap \Big[L^{\infty,2}(Q_1) \times L^{\infty,2}(\widetilde{Q}) \times L^{\infty,1}(Q) \Big]$$

and satisfies $v = v_g$ *on* $]0,T[\times\partial\Omega_1$ *and* $\theta = \theta_g$ *on* $]0,T[\times\Gamma$ *in the sense of traces, as well as the integral relations* (3.1) *and* (3.2) *for all* $\{\phi,\, \psi\} \in D^1_{s_1}(Q_1) \times \mathcal{H}^1_3(\widetilde{Q})$ *(*$s_1 > 3$*) such that* $\phi(T) = 0 = \psi(T)$*.*

Moreover, assume that there exists a Borel regular, positive Radon measure $\bar\nu \in \mathcal{M}(\overline{Q})$ *concentrated in the set* $[0,T] \times \partial\Omega_c$ *such that* $\{v,\, H,\, \theta\}$ *satisfies the integral relation* (3.10) *for all* $\xi \in W^1_{s_2,\mathcal{C}}(Q)$ *(*$s_2 > 10$*) with* $\xi(T) = 0$*. Then* $\{v,\, H,\, \theta\}$ *is called a* weak solution *to* **(P)** *with* defect measure $\bar\nu$*.*

The following existence theorem was proved in [5] under the simplifying assumption $\theta_g =$ constant. Its extension to sufficiently regular given boundary temperatures is a technical exercise.

Theorem 3.2 *Suppose that the assumptions* (3.3)*,* (3.5)*,* (3.6)*,* (3.8)*, and* (3.9) *are satisfied. Then the problem* **(P)** *possesses at least one weak solution with defect measure in the sense of Definition 3.1.*

3.2 The time-harmonic regime for the electromagnetic fields

A crystal growth process of Czochralski type takes the order of hours or days. This is an overwhelming obstacle for a complete time-dependent simulation of all quantities of interest. In this

context, it is very helpful that under certain plausible hypotheses the electromagnetic fields are in a *time harmonic regime*. This means that on the time scale of heat transport and of fluid movement in the melt these fields can be considered as *sine* functions of time having a position-dependent amplitude and phase shift, and a quite small time period of the oscillations. We assume that the given current density has the simple form of an alternating current,

$$j_g(t,x) = \sin(\omega\, t + \beta)\, j_g(x) \quad \text{in } (0,T) \times \widetilde{\Omega}_{c_0}\,, \tag{3.14}$$

where, β denotes the *phase shift*, which is constant on each subdomain of $\widetilde{\Omega}_{c_0}$. This assumption makes it possible to model the generation of traveling magnetic fields.

We make the following additional assumptions:

1. The applied alternating current j_g has a characteristic frequency $\omega > 0$ such that the corresponding time period is smaller than the typical relaxation times for momentum and heat transfer. On the time scale of the electromagnetic evolution, for example, on the interval $(t,\, t + 2\,\pi/\omega)$, the quantities v, p and θ are very close to being stationary.

2. Sufficiently far away from the beginning of the evolution, the electromagnetic fields are independent of the initial conditions, and they all reach a *time-harmonic regime*. On the time scale of momentum balance and energy balance, this happens almost immediately.

Due to the hypotheses, we can average the equations (2.1) and (2.7) over the interval $(t,\, t + 2\,\pi/\omega)$ to obtain the same equations just with $j \times B$ and $\frac{|j|^2}{\mathfrak{s}(\theta)}$ replaced by

$$[j \times B]_{\text{av}} := \frac{\omega}{2\,\pi} \int_t^{t+2\,\pi/\omega} (j \times B)\, ds\,, \tag{3.15}$$

$$\left[\frac{|j|^2}{\mathfrak{s}(\theta)}\right]_{\text{av}} := \frac{\omega}{2\,\pi} \int_t^{t+2\,\pi/\omega} \frac{|j|^2}{\mathfrak{s}(\theta)}\, ds\,, \tag{3.16}$$

respectively.

Moreover, owing to the second hypothesis, we have

$$j(t,\, x) = \operatorname{Im}(j(x)\, \exp(i\,\omega\, t)), \quad H(t,\, x) = \operatorname{Im}(H(x)\, \exp(i\,\omega\, t))\,,$$

and so on for the other electromagnetic quantities, where $j(x)$, $H(x)$ are *complex-valued* vector fields, called the *amplitudes* of the time-harmonic fields $j(t,x)$, $H(t,x)$. It follows that

$$[j \times B]_{\text{av}} = 1/2\, (\operatorname{Re}(j(x)) \times \operatorname{Re}(B(x)) + \operatorname{Im}(j(x)) \times \operatorname{Im}(B(x)))\,, \tag{3.17a}$$

$$\left[\frac{|j|^2}{\mathfrak{s}}\right]_{\text{av}} = \frac{|\operatorname{Re}(j(x))|^2 + |\operatorname{Im}(j(x))|^2}{2\,\mathfrak{s}(\theta)}\,. \tag{3.17b}$$

In the time-harmonic setting, the relation (2.17) yields $\operatorname{curl} E + i\,\omega\, B = 0$, whereas the other Maxwell's relations, which are linear and free of time derivatives, are valid for the fields j, H, E.

3.3 The quasistationary approach

Considering the equations (2.1) and (2.7) with $j \times B$ and $\frac{|j|^2}{\mathfrak{s}(\theta)}$ replaced by the time averages, and using afterwards (3.17) to compute the averages, one realizes that the stationary versions of (2.1) and (2.7) are

$$\begin{aligned} \rho_1 \, (v \cdot \nabla) v &= -\nabla p + \operatorname{div}(2\,\eta(\theta)\, D\, v) + f(\theta) + [j \times B]_{\mathsf{av}}\,, \\ \rho_1 \, c_V \, v \cdot \nabla \theta &= \operatorname{div}(\kappa(\theta)\, \nabla \theta) + \left[\frac{|j|^2}{\mathfrak{s}(\theta)}\right]_{\mathsf{av}}\,. \end{aligned} \tag{3.18}$$

The quasistationary version of the problem **(P)** also admits weak solutions. It is not the right place here to enter into the details. The core of the argumentation is the same as that for the stationary system (see [7]). A condensed version of the result is available in [8], which was followed closely for the exposition here. Note that we just need $j_g \in [L^2(\widetilde{\Omega}_{c_0})]^3$ for the proof, so that it is also allowed for a piecewise constant phase shift like in (3.14).

3.4 Optimal control theory

Since our main interest in the field of optimal control theory concentrated on the establishment of rigorous first-order optimality conditions, we decided for the paper [10] to simplify the problem in such a way that we could expect a differentiable control-to-state mapping, meaning: we considered the quasi-static case described above, with no melt motion ($v = 0$), and without dependence of the electrical conductivity on temperature ($\mathfrak{s} = \mathfrak{s}(x)$). Note that under these assumptions the corresponding Maxwell equations can be solved independently for a given current source j_g. Pairs $H,\, \theta$ of weak solutions satisfy for suitable test functions $\psi,\, \xi$ the relations

$$\begin{aligned} i \int_{\widetilde{\Omega}} \omega\, \mu(x)\, H \cdot \overline{\psi} + \int_{\widetilde{\Omega}_c} \mathfrak{s}^{-1}(x)\, \operatorname{curl} H \cdot \overline{\operatorname{curl} \psi} &= \int_{\widetilde{\Omega}_c} \mathfrak{s}^{-1}(x)\, j_g \cdot \overline{\operatorname{curl} \psi}\,, \\ \int_{\Omega} \kappa(\theta)\, \nabla \theta \cdot \nabla \xi + \int_{\Sigma} G(\sigma\, \theta^4)\, \xi &= \frac{1}{2} \int_{\Omega_c} \mathfrak{s}^{-1}(x)\, |\operatorname{curl} H|^2\, \xi\,, \end{aligned} \tag{3.19}$$

where the superscript $\bar{\cdot}$ means complex conjugation.

One essential point for the analysis of the optimal control problem is to prove that the variable θ in (3.19) is continuous and bounded in Ω. To guarantee this, we need to know that the solution H to the quasistationary Maxwell system satisfies $|\operatorname{curl} H|^2 \in L^r(\Omega)$ for some $r > 3/2$. This regularity property was proved in [10], and it represents an interesting advance in the field of regularity theory for the Maxwell system. Once that higher integrability of $\operatorname{curl} H$ is available, recent advances in the regularity theory of elliptic equations imply that the weak solution to the heat equation with nonlocal radiation boundary conditions belongs to $W^{1,q}(\Omega)$ for some $q > 3$, which is even more than Hölder continuity.

Let us only point out the additional assumptions on geometry and coefficients that are needed in this case. For the regularity of the magnetic field, the main geometrical restriction considered throughout the paper is the following:

$$\partial\widetilde{\Omega}_i \in \mathcal{C}^1, \text{ for } i = 0, \ldots, m\,, \quad \partial\widetilde{\Omega} \in \mathcal{C}^{0,1}\,. \tag{3.20}$$

We moreover assume that the conductors are isolated from each other,

$$\operatorname{dist}(\widetilde{\Omega}_i, \widetilde{\Omega}_j) > 0 \text{ for all } \widetilde{\Omega}_i,\ \widetilde{\Omega}_j \subseteq \widetilde{\Omega}_c,\ \widetilde{\Omega}_j \neq \widetilde{\Omega}_j\,. \tag{3.21}$$

In addition, we require the uniform continuity of the coefficients in each material, i. e.,

$$\mathfrak{s}_i,\ \mu_i \in C(\overline{\widetilde{\Omega}_i})\,, \tag{3.22}$$

where $\mathfrak{s}_i,\ \mu_i$ are the restrictions of $\mathfrak{s},\ \mu$ to the set $\widetilde{\Omega}_i$.

For the regularity of temperature, the same kind of hypothesis is needed, i. e.,

$$\partial\Omega_i \in \mathcal{C}^1, \quad \kappa_i \in C(\mathbb{R}^+), \qquad \text{for } i = 0, \ldots, m\,. \tag{3.23}$$

We have the following result (see [10]).

Theorem 3.3 *Suppose that the assumptions* (3.20)*,* (3.21)*,* (3.22)*, and* (3.23) *are satisfied. Then there is some* $q > 3$ *such that the control-to-state mapping* $S : j_g \mapsto \{\theta,\ H\}$ *is well defined and continuous from* $[L^q(\widetilde{\Omega}_{c_0})]^3$ *into* $W^{1,q}(\Omega) \times L^q_{\mathrm{curl}}(\widetilde{\Omega})$*.*

Another important advance established in [10] is a uniqueness result for the linearized system, which exploits techniques developed in [19] to handle the nonlinear radiation operator. We cannot enter into the details of this rather technical estimate here.

On the basis of these two results, and using techniques from standard optimal control theory, it was possible to perform a rigorous derivation of the adjoint system associated with the first-order optimality conditions under state constraints. For details, we refer the reader to [10].

4 Numerical simulations

4.1 General remarks

The numerical results presented in this section were already published in a slightly different form in [16]. We considered a growth vessel (an “LPA MARK 3”) for the LEC growth of GaAs crystals, see the left-hand side of Fig. 1. The crucible contained $4\,\mathrm{kg}$ of GaAs melt having a diameter of $15.2\,\mathrm{cm}$ and a height of $4.5\,\mathrm{cm}$. The GaAs melt was covered by a boric oxide layer of height $1.35\,\mathrm{cm}$ that was assumed to be opaque.

4.2 Global simulation of an LEC growth configuration

The electromagnetic quantities and the temperature distribution in the entire pressure chamber were computed with the software package `WIAS-HiTNIHS`, using an axisymmetric approximation of the growth vessel [15, 20, 17]. For the stationary energy balance, heat conduction and radiative heat transfer between surfaces of cavities were taken into account.

We considered the time-harmonic setting considered in section 3.2 and assumed the electromagnetic fields to be axisymmetric [20]. Accordingly, we use in the following cylindrical coordinates (r, γ, z), with the corresponding unit vectors e_r, e_γ, e_z, and the complex representation of sinusoidal functions.

In [3, 23] it was shown that under these assumptions Maxwell's equations and Ohm's law allow to find a complex-valued function $\phi(r,z)$ such that

$$A = e^{i\omega t}\phi(r,z)e_\gamma,$$

where A is the complex representation of the magnetic vector potential A introduced in section 2.5.

The electric current j has the form $j = j_\gamma \vec{e}_\gamma$, and ϕ and j_γ are computed from the following reformulation of (2.23):

$$-\nu\,\mathrm{div}\left(\frac{\mathrm{grad}(r\phi)}{r^2}\right) = \frac{j_\gamma}{r}, \quad j_\gamma = \begin{cases} 0 & \text{in the insulators,} \\ -\mathrm{i}\,\omega\,\mathfrak{s}\,\phi + \frac{\mathfrak{s}\,v_k}{2\pi r} & \text{in the } k\text{-th coil ring,} \\ -\mathrm{i}\,\omega\,\mathfrak{s}\,\phi & \text{in the other conductors.} \end{cases} \tag{4.24}$$

Here, $\nu = 1/\mu$ is the inverse of the magnetic permeability, the angular frequency of the applied voltage has the value $\omega = 2\,\pi\,300\,\mathrm{rad/s}$, and v_k is the voltage applied to the k-th coil ring. Following [17, Sec. II], we determine v_k in such a way that the total current is the same in all coil rings belonging to the same coil.

The software package `WIAS-HiTNIHS` employed for the numerical simulations is based on the finite volume method and was implemented in the framework of the program package pdelib (see [13]). It uses the grid generator Triangle (see [27]) and the sparse matrix solver PARDISO (see [26]).

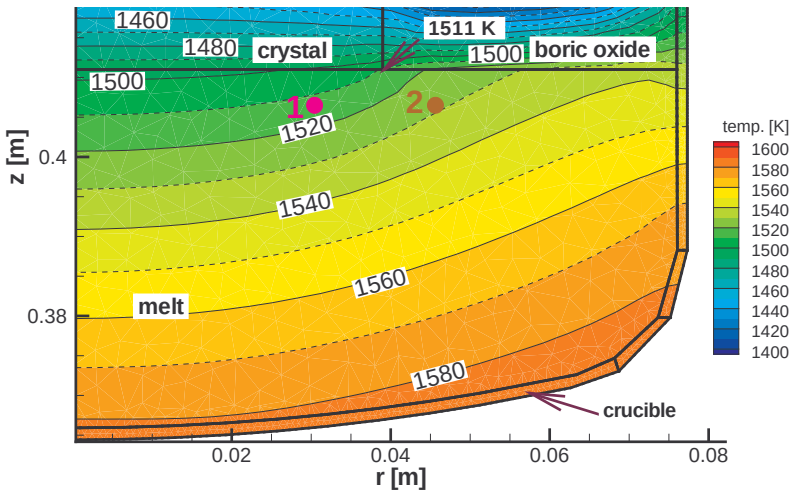

Figure 2: Global temperature distribution evaluated in melt, crystal boric oxide encapsulation, and crucible in the considered LEC configuration. The solid isotherms are spaced at $20\,\mathrm{K}$, the dotted isotherms in between at $10\,\mathrm{K}$. The points "1" (purple) and "2" (brown) mark the monitor points used in the following analysis of the temperature oscillations.

The total input power P was adjusted in such a way that the given trijunction between melt, crystal, and boric oxide was maintained at the melting temperature of GaAs ($1511\,\mathrm{K}$), leading to a power request of $6.97\,\mathrm{kW}$. Fig. 2 shows the global temperature distribution in the vicinity of the melt.

In the temperature computation the heat transport due to gas convection was neglected. Therefore, the required input power was lower than in the real system. To compensate for this underestimation, while computing the Lorentz force, the input power was increased to approximately $10.5\,\mathrm{kW}$.

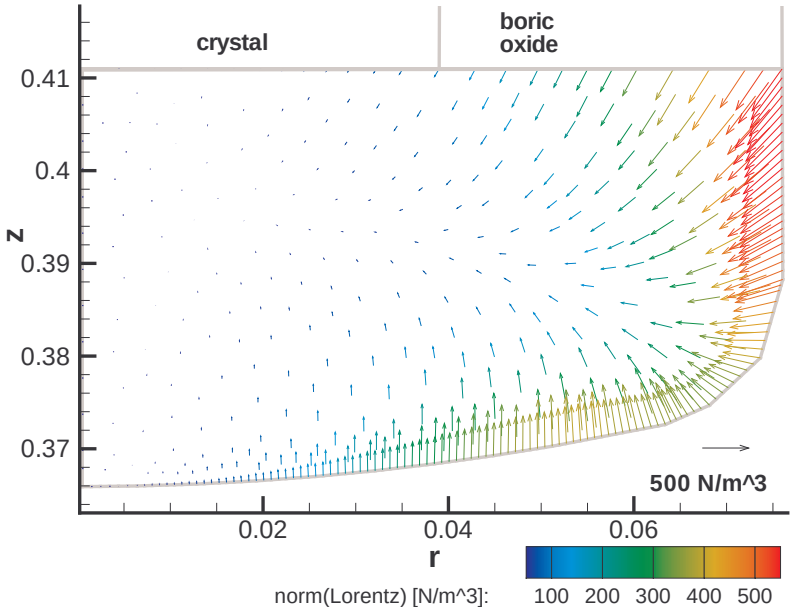

Figure 3: Lorentz force density in the melt. The reference vector corresponds to a force density of $500\,\mathrm{N}/\,\mathrm{m}^3$. The maximum of the density is about $570\,\mathrm{N}/\,\mathrm{m}^3$.

The HMM consisted of three vertically placed coils surrounding the crucible. These coils generated a downwards moving TMF with a phase shift of 70° between the voltages applied to them. Following patent [12], these coils were combined with two additional coils below the crucible, see Fig. 1. These coils generated an additional outward moving TMF, also with a phase shift of 70°.

The resulting Lorentz force density is depicted in Fig. 3. This density is maximal close to the side wall of the crucible. Because of coils placed below the crucible (following patent [12]), the Lorentz force also acted with comparable strength halfway inwards at the bottom of the crucible, see [16].

4.3 Local simulation of an LEC growth configuration

In the melt, we solved the transient Navier-Stokes equations ((2.1) and (2.2)), together with the energy equation ((2.7)) in Boussinesq approximation:

$$\begin{aligned} \partial_t u + (u\cdot\nabla)u + \nabla p &= \frac{1}{\mathrm{Re}}\triangle u + \frac{\mathrm{Gr}}{\mathrm{Re}^2} T\, e_z + \frac{L}{\rho_0 V^2} F_\mathrm{L}\,, \\ \nabla\cdot u = 0, \qquad \partial_t T + (u\cdot\nabla)T &= \frac{1}{\mathrm{Re}\,\mathrm{Pr}}\triangle T\,. \end{aligned} \tag{4.25}$$

Here, u, p, and T denote the dimensionless velocity, pressure, and temperature. The radius

$R_c = 7.6\,\mathrm{cm}$ of the crucible was taken as the length scale, and the scale for the velocity was $V = \Omega_X R_c = 3.98\,\mathrm{cm/s}$, with $\Omega_X = 5\,\mathrm{rpm}$ being the rotation rate of the crystal.

Moreover, for GaAs with a kinematic viscosity $\nu = \frac{\eta}{\rho_1} = 0.00488\,\mathrm{cm^2/s}$ and a thermal expansion coefficient $\alpha = 0.0001867\,1/\mathrm{K}$, the corresponding *Reynolds number* was $\mathrm{Re} = \frac{R_c V}{\nu} = 6.197 \times 10^3$ and, for typical temperature differences δT of 30 K occurring in the melt, the *Grashof number* was $\mathrm{Gr} = \frac{\alpha\,\delta T\,R_c^3\,g}{\nu^2} = 1.013 \times 10^8$, where g denotes the gravitational acceleration.

Furthermore, the density of the GaAs melt at the melting temperature $1511\,\mathrm{K}$ is $\rho_1 = 5.71323 \times 10^3\,\mathrm{kg/m^3}$, the specific heat is $c_{V1} = 434\,\frac{\mathrm{J}}{\mathrm{kg\ K}}$, and the thermal conductivity is $\kappa_1 = 0.178\,\frac{\mathrm{W}}{\mathrm{cm\ K}}$. Hence, the *Prandtl number* resulted to $\mathrm{Pr} = \frac{\nu\,\rho_1\,c_{V1}}{\kappa_1} = 0.068$. The Lorentz force density F_L was taken from the global simulation.

The axisymmetric numerical simulations were performed with the finite element code NAVIER developed by E. Bänsch [2]. We used a time step size of $0.00141\,\mathrm{s}$ and a grid with 27032 triangles. The boundary conditions for temperature (respectively, normal heat flux) in the melt were taken from the global simulation, see [20, 15]. In order to numerically investigate the effect of the Lorentz force vs. buoyancy, we kept the crucible at the (low) rotation rate of $\Omega_C = -5\,\mathrm{rpm}$.

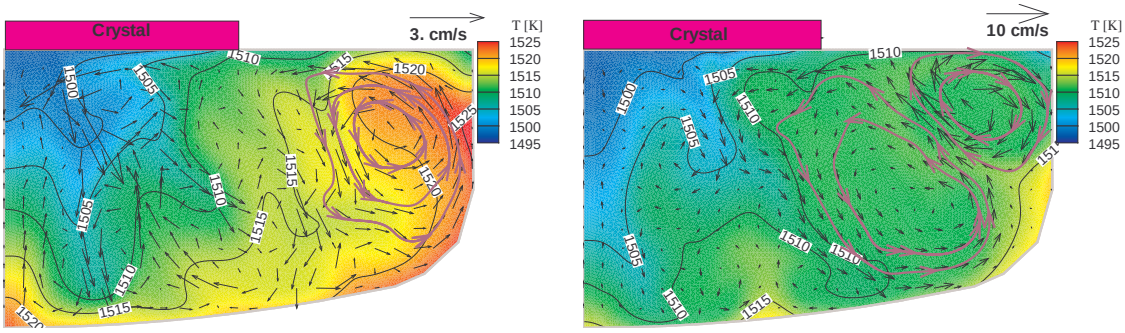

Figure 4: Snapshots of velocity and temperature distribution from the local simulation of the LEC configuration without Lorentz force (left-hand side) and with the Lorentz force from Fig. 3 (right-hand side). Note the different velocity scales.

Fig. 4 shows snapshots of velocity and temperature distribution in the melt without the action of a Lorentz force (left) and with the Lorentz force shown in Fig. 3 (right). The snapshot shown on the left-hand side of Fig. 4 reveals that the natural convection due to buoyancy generates an inward-rotating roll near to the crucible wall (right-hand side of the melt). This roll is partially suppressed by the Lorentz force, which generates in the upper outer part of the melt an outward-rotating toroidal roll. An additional (non-permanent) counter-rotating roll seems to provide for a better mixing of temperature in the melt down to the middle radius.

This is also reflected in the temperature variations close to the trijunction point. Figs. 5 and 6 show the temperature oscillations in two points (marked by “1” and “2” in Fig. 2). In both points, the amplitude of the low frequency temperature oscillations is reduced by the application of the TMF.

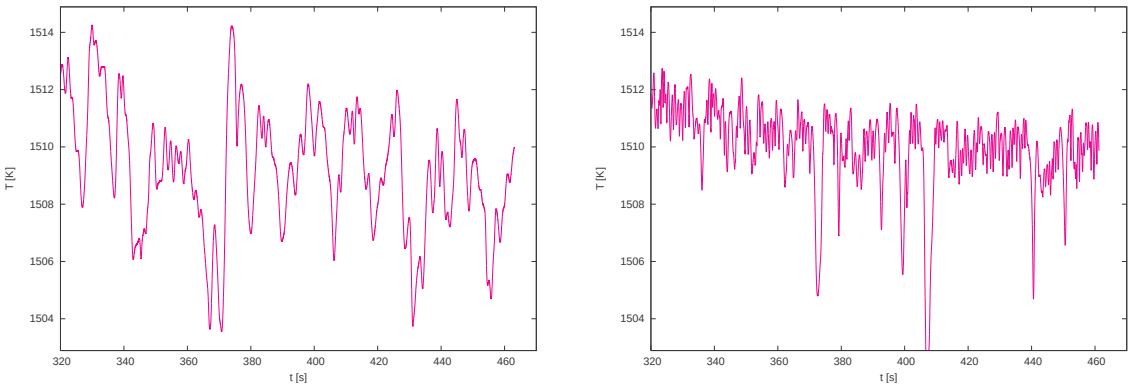

Figure 5: Temperature oscillations in the monitor point “1” from the local simulation of the LEC configuration without Lorentz force (left-hand side) and with the Lorentz force from Fig. 3 (right-hand side).

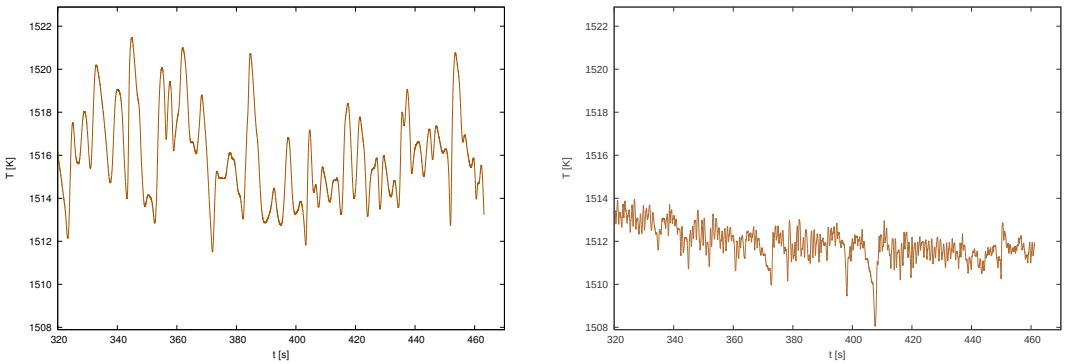

Figure 6: Temperature oscillations in the monitor point “2” from the local simulation of the LEC configuration without Lorentz force (left-hand side) and with the Lorentz force of Fig. 3 (right-hand side).

References

[1] A. Bossavit, *Electromagnétisme en vue de la Modélisation*, Springer, Berlin–Heidelberg–New York 2004.

[2] E. Bänsch. *Simulation of instationary, incompressible flows*, Acta Mathematica Universitatis Comenianae, vol. **LXVII** (1998), pp. 101 –114.

[3] S. Clain, J. Rappaz, and M. Swierkosz, *Coupling between nonlinear Maxwell and heat equations for an induction heating problem: Modeling and numerical methods*, Krizek, M. (ed.) et al., Finite element methods. 50 years of the Courant element. Conference held at the Univ. of Jyvaeskylae, Finland, 1993. New York, NY: Marcel Dekker, Inc. Lect. Notes Pure Appl. Math. 164, 163-171 (1994).

[4] P.-É. Druet, *Weak solutions to a stationary heat equation with nonlocal radiation boundary condition and right-hand side in* L^p , Math. Meth. Appl. Sci. **32** (2008), 135–166.

[5] P.-É. Druet, *Existence of weak solutions to the time-dependent MHD equations coupled to the heat equation with nonlocal radiation boundary conditions*, Nonlin. Anal. RWA **10** (2009), 2914–2936.

[6] P.-É. Druet, *Analysis of a coupled system of partial differential equations modeling the interaction between melt flow, global heat transfer and applied magnetic fields in crystal growth*, PhD Thesis, Humboldt-Universität zu Berlin, 2009.

[7] P.-É. Druet, *Existence for the stationary MHD-equations coupled to heat transfer with nonlocal radiation effects*, Cz. Math. J. **59** (2009), 791–825.

[8] P.-É. Druet, *Weak solutions to a model for crystal growth from the melt in changing magnetic fields*, in: (K. Kunisch, G. Leugering, J. Sprekels and F. Tröltzsch, eds.), Öptimal Control of Coupled Systems of PDE", International Series of Numerical Mathematics **158** (2009), Basel, Birkhäuser, 123–137.

[9] P.-É. Druet, *Weak solutions to a time-dependent heat equation with nonlocal radiation boundary condition and arbitrary p-summable right-hand side*, Appl. of Math. **55** (2010), 111–149.

[10] P.-É. Druet, O. Klein, J. Sprekels, F. Tröltzsch, and I. Yousept, *Optimal control of three-dimensional state-constrained induction heating problems with nonlocal radiation effects*, SIAM J. Control Optim. **49** (2011), 1707–1736.

[11] P.-É. Druet and P. Philip, *Noncompactness of integral operators modeling diffuse-gray radiation in polyhedral and transient settings*, Integr. Equ. Oper. Theory **69** (2011), 101–111.

[12] C. Frank-Rotsch, et al. *Vorrichtung und Verfahren zur Herstellung von Kristallen aus elektrisch leitenden Schmelzen (Device and method for producing crystals from electroconductive melt)*, July, 17th, 2009, Patentschrift (patent specification) of granted german patent 10 2007 028 548, German Patent and Trade Mark Office, December, 21st, 2011, patent specification of granted european patent EP 2 162 571 B1, European Patent Office.

[13] J. Fuhrmann, T. Koprucki, and H. Langmach, *pdelib: An open modular toolbox for the numerical solution of partial differential equations. design patterns*, In W. Hackbusch and G. Wittum, Editors, Proceedings of the 14th GAMM Seminar on Concepts of Numerical Software (University of Kiel, 2001), pp. 121 – 132.

[14] O. Klein, P. Philip, and J. Sprekels, *Modelling and simulation of sublimation growth in SiC bulk single crystals*, Interfaces Free Bound. **6** (2004), 295–314.

[15] O. Klein, Ch. Lechner, P.-É. Druet, P. Philip, J. Sprekels, Ch. Frank-Rotsch, F. M. Kießling, W. Miller, U. Rehse, and P. Rudolph, *Numerical simulation of Czochralski crystal growth under the influence of a traveling magnetic field generated by an internal heater-magnet module (HMM)*, J. Crystal Growth **310** (2008), 1523–1532.

[16] O.Klein, C. Lechner, P.-É. Druet, P. Philip, J. Sprekels, C. Frank-Rotsch, F.-M. Kießling, W. Miller, U. Rehse, P. Rudolph, *Numerical simulations of the influence of a traveling magnetic*

field, generated by an internal heater-magnet module, on liquid encapsulated Czochralski crystal growth, Magnetohydrodynamics **45** (2009), 557–567.

[17] O. Klein, P. Philip, *Correct voltage distribution for axisymmetric sinusoidal modeling of induction heating with prescribed current, voltage, or power*, IEEE Transactions on Magnetics **38** (2002), 1519–1523.

[18] O. Klein, P. Philip, *Transient conductive-radiative heat transfer: Discrete existence and uniqueness for a finite volume scheme*, Math. Models Methods Appl. Sci. **15** (2005), 227–258.

[19] M. Laitinen, T. Tiihonen, *Conductive-radiative heat transfer in grey materials*, Quart. Appl. Math. **59** (2001), 737–768.

[20] C. Lechner, O. Klein, P.-É. Druet, *Development of a software for the numerical simulation of VCz growth under the influence of a traveling magnetic field*, J. Crystal Growth **303** (2007), 161–164.

[21] C. Meyer, P. Philip, and F. Tröltzsch, *Optimal control of a semilinear PDE with nonlocal radiation interface conditions*, SIAM J. Control Optim. **45** (2006), 699–721.

[22] C. Meyer and I. Yousept, *Regularization of state-constrained optimal control of semilinear elliptic equations with nonlocal radiation interface conditions*, SIAM J. Control Optim. **48** (2009), 734–755.

[23] J. Rappaz and M. Swierkosz *Modelling in numerical simulation of electromagnetic heating*, Modelling and optimization of distributed parameter systems (Warsaw, 1995), Chapman & Hall, New York, 1996, 313–320,

[24] P. Rudolph, *Travelling magnetic fields applied to bulk crystal growth from the melt:The step from basic research to industrial scale*, J. Crystal Growth **310** (2008), 1298–1306.

[25] P. Rudolph, Ch. Frank-Rotsch, F.-M. Kiessling, W. Miller, U. Rehse, O. Klein, Ch. Lechner, J. Sprekels, B. Nacke, H. Kasjanov, P. Lange, M. Ziem, B. Lux, M. Czupalla, O. Root, V. Trautmann, G. Bethin, *Crystal growth in heater-magnet modules – From concept to use*, in: (E. Braake, B. Nacke, eds.), "Proceedings of the International Scientific Colloquium Modelling for Electromagnetic Processing (MEP2008), Hannover, October 26-29, 2008", Leibniz University of Hannover (2008), 26–29.

[26] O. Schenk and K. Gärtner, *Solving unsymmetric sparse systems of linear equations with pardiso*. Journal of Future Generation Computer Systems **20** (2004), no. 3, pp. 475–487.

[27] J. Shewchuk. *Triangle: Engineering a 2d quality mesh generator and delaunay triangulator.* In *First Workshop on Applied Computational Geometry (Philadelphia, Pennsylvania)* (ACM, 1996), pp. 124–133.